

Article

Wavelength Dependence of the Photocatalytic Performance of Pure and Doped TiO₂ Photocatalysts—A Reflection on the Importance of UV Excitability

Gábor Veréb ^{1,*} , Tamás Gyulavári ² , Orsolya Virág ¹, Tünde Alapi ³ , Klara Hernadi ^{2,4}  and Zsolt Pap ^{2,5,6,*}

- ¹ Department of Biosystems Engineering, Faculty of Engineering, University of Szeged, Moszkvai Blvd. 9, H-6725 Szeged, Hungary
- ² Department of Applied and Environmental Chemistry, University of Szeged, Rerrich Béla Sqr. 1, H-6720 Szeged, Hungary
- ³ Department of Inorganic and Analytical Chemistry, Institute of Chemistry, University of Szeged, Dóm Sqr. 7, H-6720 Szeged, Hungary
- ⁴ Institute of Physical Metallurgy, Metal Forming and Nanotechnology, University of Miskolc, Miskolc-Egyetemváros, C/1 108, H-3515 Miskolc, Hungary
- ⁵ Nanostructured Materials and Bio-Nano-Interfaces Center, Interdisciplinary Research Institute on Bio-Nano-Sciences, Babes-Bolyai University, Treboniu Laurian 42, RO-400271 Cluj-Napoca, Romania
- ⁶ Institute of Research-Development-Innovation in Applied Natural Sciences, Babes-Bolyai University, Fântânele Str. 30, RO-400294 Cluj-Napoca, Romania
- * Correspondence: verebg@mk.u-szeged.hu (G.V.); pzsolt@chem.u-szeged.hu (Z.P.); Tel.: +36-62-546-582 (G.V.); +36-62-543-795 (Z.P.)



Citation: Veréb, G.; Gyulavári, T.; Virág, O.; Alapi, T.; Hernadi, K.; Pap, Z. Wavelength Dependence of the Photocatalytic Performance of Pure and Doped TiO₂ Photocatalysts—A Reflection on the Importance of UV Excitability. *Catalysts* **2022**, *12*, 1492. <https://doi.org/10.3390/catal12121492>

Academic Editors: Amr Fouda and Mohammed F. Hamza

Received: 18 October 2022

Accepted: 9 November 2022

Published: 22 November 2022

Publisher's Note: MDPI stays neutral with regard to jurisdictional claims in published maps and institutional affiliations.



Copyright: © 2022 by the authors. Licensee MDPI, Basel, Switzerland. This article is an open access article distributed under the terms and conditions of the Creative Commons Attribution (CC BY) license (<https://creativecommons.org/licenses/by/4.0/>).

Abstract: The photocatalytic performances of doped and non-doped TiO₂ photocatalysts (TiO₂-s) were compared under solar and various types of artificial irradiation using phenol as a model contaminant. Non-doped (mainly anatase phase) TiO₂-s had significantly higher photocatalytic efficiency than highly visible-light-active TiO₂-s under natural solar irradiation. To explain these unexpected results, we measured the wavelength dependence of photocatalytic efficiency at six different wavelength ranges ($\lambda = 300\text{--}650$ nm). For this purpose, UV fluorescence tubes and five LED lights of different colors (violet, blue, green, yellow, and red) were used to activate the photocatalysts. The photon fluxes of the irradiation were measured, and apparent quantum yields were calculated for all irradiation conditions. The highest apparent quantum yield was 1.43% for our own TiO₂ (prepared via flame hydrolysis) under UV irradiation. However, apparent quantum yields were significantly lower (by 1–2 orders of magnitude) in the visible range, even for the most visible-light-active TiO₂.

Keywords: TiO₂; visible light; UV light; solar irradiation; apparent quantum yield

1. Introduction

Heterogeneous photocatalysis is a widely used technology in the development of several novel water purification processes [1,2]. It can be used to degrade hazardous organic materials [3–6], prepare self-cleaning and solar-cleanable membrane surfaces used in membrane photoreactors [7–9], or produce green energy sources from organic pollutants [10–13]. Moreover, the utilization of photocatalytic nanomaterials is not limited to water purification; they are essential in the development of air-cleaning processes [1,14,15], self-cleaning surfaces [16–18], photocatalytic water splitting [19,20], and artificial photosynthesis [21,22].

TiO₂ is the most widely investigated photocatalyst because of its numerous favorable properties. To name a few, it is photostable, biologically inert, available in large quantities, and non-toxic [2,23–25]. While its photocatalytic activity mostly depends on its own characteristic properties (crystal phase, doping elements, surface properties, particle size and shape, etc.), there are other factors that significantly affect the photocatalytic efficiency: (a) the nature and concentration of the target contaminant, which determine the interactions between

the substrate and the nanoparticle [26]; (b) the intensity of irradiation (the photon flux or photon density), which determines the formation rate of charge carriers and has an impact on their lifetime (which limits their availability for redox reactions on the surface) [27,28]; and (c) probably most importantly, the wavelength of the used irradiation [29,30].

It is well-known that undoped TiO₂-s can be excited mainly by UV photons (specifically, anatase, rutile, and brookite have band gaps of 387 [1,2,16], 410 [31], and 419 nm [31], respectively). This is a very unfavorable property for novel solar light-based technologies, as only 3–6% of the solar photons are in the UV range [32–35]. The light intensity of sunlight is about ten times higher in the visible range (~45% of the solar spectra [14,16]). Therefore, many researchers have sought to develop visible-light-active photocatalysts, which are expected to improve solar light utilization [1,2,16,24,32–37]. Nitrogen [2,24,25,36–43], sulphur [1,37,38,44], iodine [45–48], iron [1,23,40], phosphorus [33,49], tungsten [2,50], and numerous other elements have been successfully applied as doping elements, resulting in increased visible light excitability. However, their sunlight-induced photocatalytic efficiencies, which are expected to improve, have not been investigated with outdoor solar experiments in most cases. Moreover, authors have reported lower solar photocatalytic efficiencies for highly visible-light-active photocatalysts than for pure titanium dioxides. For example, Wang et al. [43] reported significantly higher solar phenol decomposition efficiency for Aerioxide P25 than that for the visible-light-active TiO₂ they made. Rengifo-Herrera and Pulgarin [38] determined more effective solar disinfection efficiency for pure TiO₂ than for their doped visible-light-active TiO₂-s. Nascimben Santos et al. [7] reported higher photocatalytic flux recovery for pure TiO₂-covered membranes than that for visible-light-active membranes during solar photocatalytic membrane regeneration. These results highlight the necessity of a detailed experiment in which the photocatalytic efficiencies of highly UV- and visible-light-active photocatalysts are compared under different kinds of irradiation.

In an earlier study, the visible light excitability of ten different TiO₂-based photocatalysts was investigated [41]. Out of these, the three most active TiO₂-s were selected to be investigated in the present study. The photocatalytic performance of visible-light-active TiO₂-s (Kronos VLP7000, Aldrich rutile, and a nitrogen-doped TiO₂) and non-doped mainly anatase phase TiO₂-s (Aerioxide P25, Aldrich anatase, and another non-doped TiO₂ that was synthesized via flame hydrolysis) were compared under solar irradiation. The results point out that high visible light excitability is not a guarantee of better solar light utilization. To explain these results, we investigated the wavelength dependence of the photocatalysts. Apparent quantum yields were determined at six different wavelength ranges for all TiO₂-s in the case of phenol decomposition. Phenol was chosen because it is a widely-used colorless model contaminant with a concentration that can be precisely followed via high performance liquid chromatography.

2. Results and Discussion

2.1. Photocatalytic Performance

Before the investigation of photocatalytic performance, blank experiments were carried out in the dark with all the investigated TiO₂-s to measure phenol adsorption (after 120 min), which was lower than 1% in all cases. The different effects of irradiation were investigated without the addition of any photocatalyst; the measured phenol degradations were <2% in the case of UV fluorescence tubes (after 120 min) and <1% in the case of different visible light irradiation.

2.1.1. Experiments with Visible-Light-Emitting Energy-Saving Compact Fluorescence Lamps

Figure 1a demonstrates the results of visible-light-driven photocatalytic experiments, using commercial energy-saving compact fluorescence lamps for excitation. TiO₂-AA had negligible photocatalytic efficiency (<5% of phenol was decomposed after 4 h of irradiation). TiO₂-P25 showed significant efficiency (17% conversion). Much higher activity was measured for our TiO₂-N (26% decrease) and for the commercial TiO₂-AR (37% decrease),

while TiO₂-VLP7000 had by far the highest photocatalytic efficiency (94% decrease). Because the intensity of natural solar light is ten times higher in the visible range than in the UV range [14,16,32–35], it can be expected that visible-light-active TiO₂-s should be more efficient for solar photocatalytic water treatment.

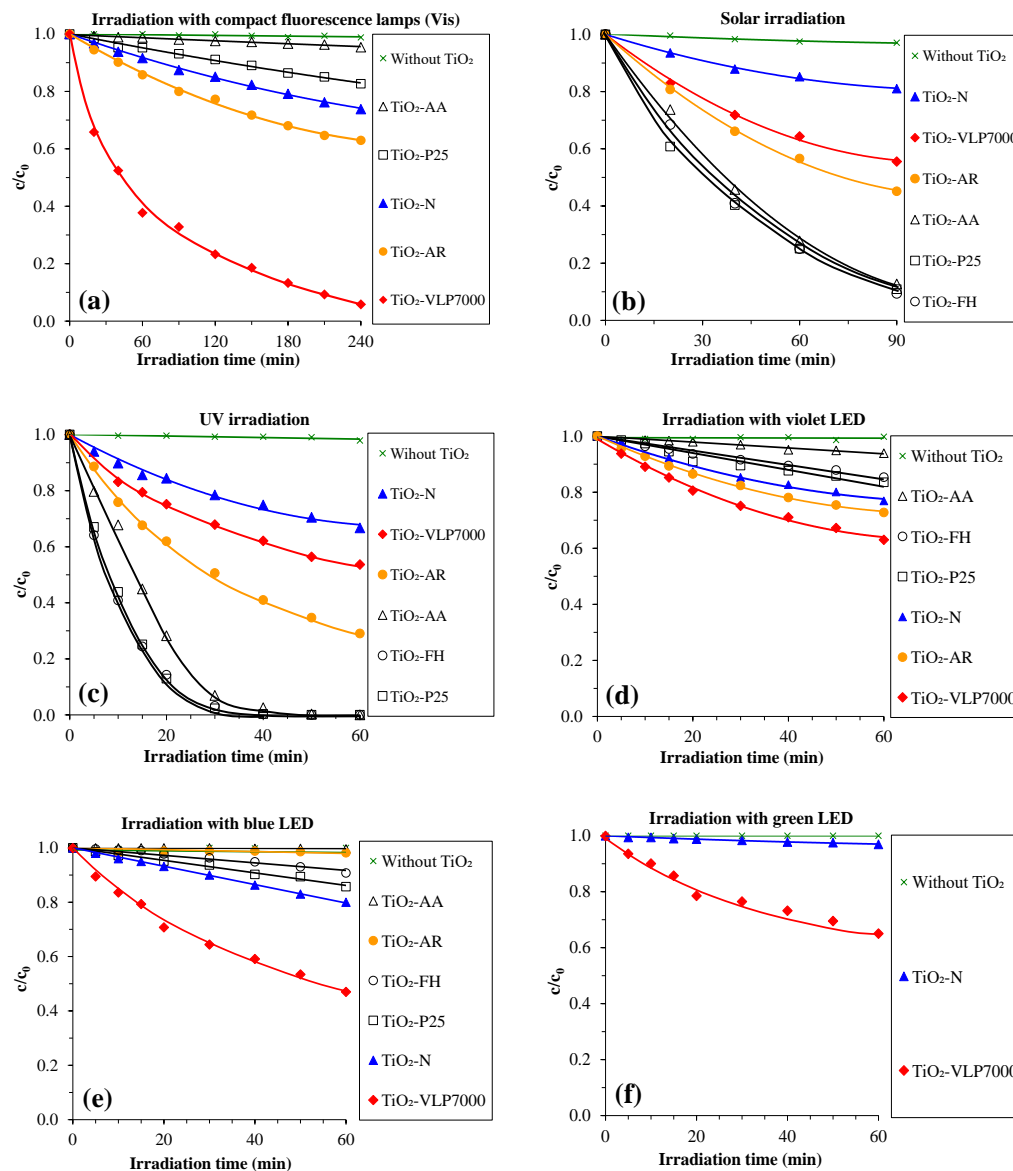


Figure 1. Photocatalytic phenol decomposition ($c_{\text{phenol}} = 0.1 \text{ mM}$, $c_{\text{TiO}_2} = 1.0 \text{ g}\cdot\text{L}^{-1}$) applying (a) energy-saving compact fluorescence lamps, (b) natural solar irradiation, (c) UV-A irradiation, (d) violet irradiation, (e) blue irradiation, and (f) green irradiation.

2.1.2. Solar Experiments

Figure 1b demonstrates the results of the outdoor solar photocatalytic experiments. Unexpectedly, non-doped mainly anatase phase TiO₂-s (TiO₂-AA, TiO₂-FH, TiO₂-P25) were twice as efficient (87–89% of phenol was decomposed after 90 min of irradiation) as TiO₂-VLP7000 (44% phenol removal), despite TiO₂-VLP7000 being the best under visible light irradiation. Moreover, non-doped Aldrich rutile was observed to be marginally better (55% degradation), while TiO₂-N showed the lowest performance (only 19% of phenol was decomposed) despite its significant visible light excitability (Figure 1a). To explain these results, we investigated the wavelength dependence of photocatalytic phenol decomposition performance in detail. For this purpose, we used UV fluorescence tubes and five different colored LED lights (violet, blue, green, yellow, and red) to activate the photocatalysts.

2.1.3. Photocatalytic Experiments with UV Lights and Different Colored LED Lights

The calculated initial phenol decomposition rates ($\text{M}\cdot\text{s}^{-1}$) are summarized in Table 1 for all TiO_2 -s at all irradiation conditions. Figure 1c shows the decay curves of UV photocatalytic experiments. The non-doped mainly anatase phase TiO_2 -s (marked with hollow symbols) had much higher photocatalytic performances under UV irradiation ($r_0 = 5.8\cdot 10^{-8}$ – $1.3\cdot 10^{-7} \text{ M}\cdot\text{s}^{-1}$) than the non-doped rutile (TiO_2 -AR; $r_0 = 3.8\cdot 10^{-8} \text{ M}\cdot\text{s}^{-1}$), doped TiO_2 -VLP7000 ($r_0 = 2.3\cdot 10^{-8} \text{ M}\cdot\text{s}^{-1}$), and TiO_2 -N ($r_0 = 1.6\cdot 10^{-8} \text{ M}\cdot\text{s}^{-1}$). The sequence of photocatalytic efficiencies was the same as in the solar experiments. The rates were very similar as well, which suggests a strong correlation between UV excitability and solar photocatalytic performance.

Table 1. Initial degradation rate of phenol ($\text{mol}\cdot\text{dm}^{-3}\cdot\text{s}^{-1}$) for different photocatalysts under different irradiations.

Irradiation Type	Initial Degradation Rate of Phenol ($\text{mol}\cdot\text{dm}^{-3}\cdot\text{s}^{-1}$)					
	TiO_2 -AA	TiO_2 -FH	TiO_2 -P25	TiO_2 -AR	TiO_2 -N	TiO_2 -VLP7000
UV	$5.8\cdot 10^{-8}$	$1.3\cdot 10^{-7}$	$1.2\cdot 10^{-7}$	$3.8\cdot 10^{-8}$	$1.6\cdot 10^{-8}$	$2.3\cdot 10^{-8}$
Violet	$1.8\cdot 10^{-9}$	$5.6\cdot 10^{-9}$	$7.0\cdot 10^{-9}$	$1.3\cdot 10^{-8}$	$1.0\cdot 10^{-8}$	$1.8\cdot 10^{-8}$
Blue	-	$1.3\cdot 10^{-9}$	$3.9\cdot 10^{-9}$	$5.7\cdot 10^{-10}$	$5.9\cdot 10^{-9}$	$2.6\cdot 10^{-8}$
Green	-	-	-	-	$8.9\cdot 10^{-10}$	$1.8\cdot 10^{-8}$
Yellow	-	-	-	-	-	$3.6\cdot 10^{-9}$
Red	-	-	-	-	-	$5.8\cdot 10^{-9}$

Under violet irradiation (Figure 1d), the non-doped mainly anatase phase TiO_2 -s (TiO_2 -AA, TiO_2 -FH, and TiO_2 -P25) showed lower performance (r_0 : 1.8 – $7.0\cdot 10^{-9} \text{ M}\cdot\text{s}^{-1}$) than doped TiO_2 -s or rutile phase TiO_2 -AR (r_0 : 1.3 – $1.8\cdot 10^{-8} \text{ M}\cdot\text{s}^{-1}$), as expected. Under blue irradiation (Figure 1e), TiO_2 -VLP7000 showed the highest photocatalytic efficiency ($r_0 = 2.6\cdot 10^{-8} \text{ M}\cdot\text{s}^{-1}$), while for TiO_2 -FH, TiO_2 -P25, and TiO_2 -N much lower phenol degradation rates were measured ($r_0 = 1.3$ – $5.9\cdot 10^{-9} \text{ M}\cdot\text{s}^{-1}$). TiO_2 -AR showed very poor (though measurable) photocatalytic efficiency ($r_0 = 5.7\cdot 10^{-10} \text{ M}\cdot\text{s}^{-1}$), while no phenol decomposition was observed for TiO_2 -AA. Under green (Figure 1f), yellow, and red irradiation, only TiO_2 -VLP7000 had notable photocatalytic performance; the values of the initial degradation rates are provided in Table 1.

2.2. Incident Photon Fluxes

For correct comparison of the measured efficiencies under different irradiations, apparent quantum yields have to be calculated; therefore, the incident photon fluxes were measured. The emission spectra of violet, blue, and green LED strips and the transmittance of 0.02 M and 0.15 M potassium-iron(III)-oxalate solutions (at 5 cm liquid thickness applied in the photoreactor) are presented in Figure 2. Incident photon fluxes for UV and violet irradiations can be measured using 0.02 M ferrioxalate solution, as it absorbs all photons at these wavelength ranges. However, it does not absorb all photons emitted by blue (or any other) LED lights (see Figure 2).

Therefore, the photon flux for blue irradiation was determined both with 0.02 M and 0.15 M iron(III)-oxalate solutions. The difference was 17.6% in favor of the 0.15 M solution, which justifies the necessity of applying a higher concentration. Calculated incident photon fluxes are shown in Table 2. The photon fluxes for green, yellow, and red irradiation were calculated with a PPF meter as described in Section 3.2.3. The calculated values are presented in Table 3.

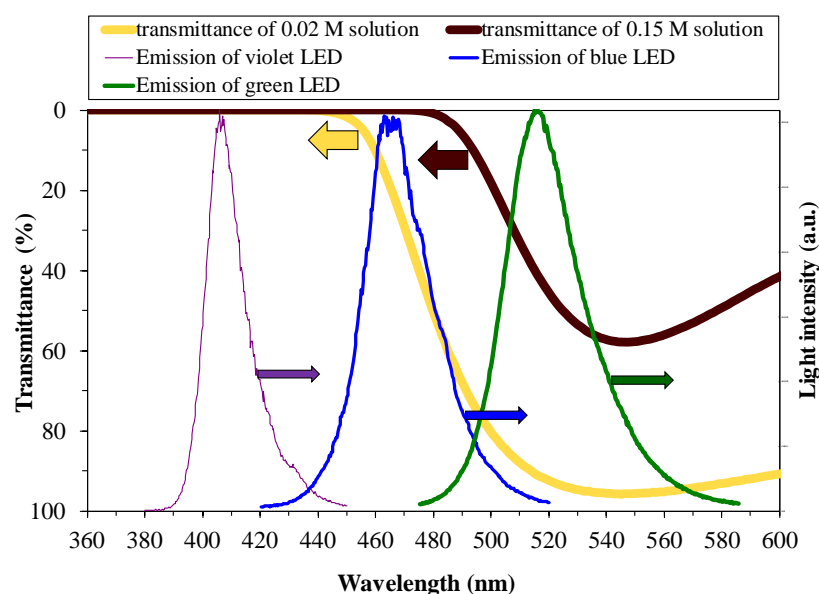


Figure 2. Emission spectra of violet, blue, and green LED strips and the transmittance spectra of 0.02 M and 0.15 M potassium iron(III) oxalate solutions.

Table 2. Incident photon fluxes determined by potassium ferrioxalate actinometry.

Irradiation	UV	Violet	Blue	
			(Using 0.02 M Fe-Oxalate Solution)	(Using 0.15 M Fe-Oxalate Solution)
Incident photon flux (mol·dm ⁻³ ·s ⁻¹)	9.23·10 ⁻⁶	7.75·10 ⁻⁶	4.25·10 ⁻⁵	5.16·10 ⁻⁵

Table 3. Incident photon fluxes under green, yellow, and red irradiation obtained from the multiplication of incident photon flux under blue irradiation (5.16·10⁻⁵ M·s⁻¹; determined by ferrioxalate actinometry) and the ratios of light intensities measured by a PPF meter.

Irradiation Type	Ratio of Photon Flux Belonging to Actual Irradiation and Photon Flux of Blue LED (Measured by PPF Meter)	Calculated Incident Photon Flux (mol·dm ⁻³ ·s ⁻¹)
blue LED	1.00	5.16·10 ⁻⁵
green LED	0.69	3.56·10 ⁻⁵
yellow LED	0.21	1.08·10 ⁻⁵
red LED	1.14	5.88·10 ⁻⁵

2.3. Discussion of the Calculated Apparent Quantum Yields

The apparent quantum yields of phenol decomposition for different TiO₂-s and different irradiation (Figure 3) were calculated by the ratio of the phenol degradation rates (mol·dm⁻³·s⁻¹) and the actual incident photon fluxes (mol·dm⁻³·s⁻¹). TiO₂-FH had the highest determined apparent quantum yield (1.43%) under UV irradiation. For Aeroxide P25, a similar value of 1.28% was calculated. On the one hand, Figure 3 shows that non-doped mainly anatase phase TiO₂-s utilize UV photons with much higher efficiency than doped TiO₂-s and Aldrich rutile (0.17–0.41% apparent quantum yields were calculated). On the other hand, much lower apparent quantum yields (0.02–0.09%) were measured in the violet range for these photocatalysts than those for Kronos VLP7000 (0.23%), TiO₂-N (0.13%), and Aldrich rutile (0.16%). Moreover, Kronos VLP7000 TiO₂ could be excited in the whole UV–vis spectra; at higher wavelengths, only this TiO₂ had notable efficiency. For non-doped anatase phase TiO₂-s, the apparent quantum yields are 1–2 order(s) of magnitude higher in the UV range than those of doped TiO₂-s in the visible range. This means that despite the increased visible light excitability, if a given catalyst utilizes UV

photons less effectively than this fact can likely overcompensate the beneficial effect of extended excitability, leading to lower overall photocatalytic performance. This results in higher performance for non-doped TiO₂-s under solar irradiation despite the one order of magnitude lower quantity of UV photons in the sunlight.

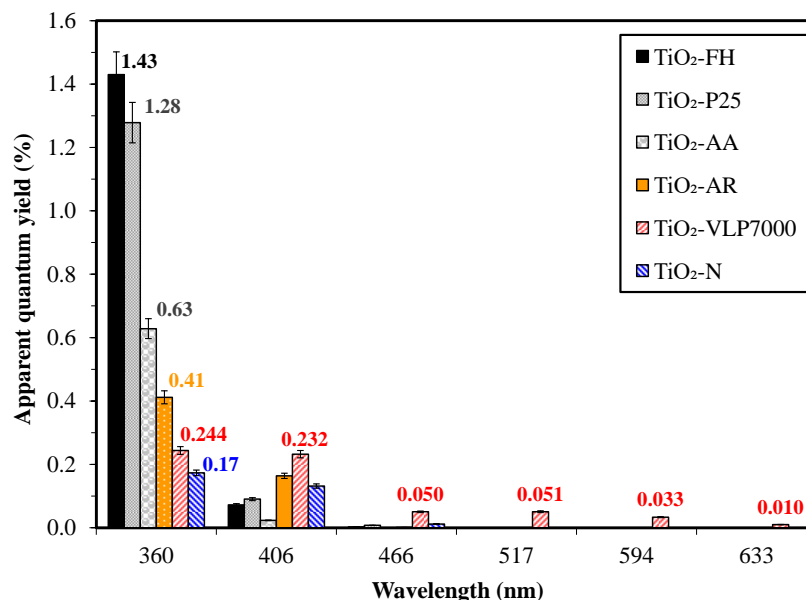


Figure 3. Apparent quantum yields for photocatalytic phenol degradation ($c = 0.1$ mM).

These results are consistent with the study of Wang et al. [43], in which Aeroxide P25 showed higher photocatalytic efficiency than their highly visible-light-active TiO₂ under solar irradiation. In addition, Emeline et al. [42] observed one order of magnitude lower quantum yield in the visible range ($400 < \lambda < 550$ nm) than in the UV-A range for their own TiO₂.

Consequently, while doped and/or rutile phase titanium dioxides can be much more efficient under visible light irradiation (e.g., for self- or air-cleaning indoor surfaces), a higher visible light activity does not necessarily lead to higher performance under solar light irradiation. If higher solar light utilization is the aim during the development of a novel photocatalyst, UV excitability is crucial, and should be investigated.

3. Materials and Methods

3.1. Materials

Photocatalytic water treatment experiments were carried out by applying phenol (Spektrum 3D, Debrecen, Hungary; analytical grade) as a model contaminant.

For potassium ferrioxalate actinometry measurements, iron sulphate (Reanal, Budapest, Hungary; analytical grade), o-phenanthroline (Reanal, Budapest, Hungary; analytical grade), potassium oxalate (Spektrum 3D, Debrecen, Hungary; 99.5%), sodium acetate (Spektrum 3D, Debrecen, Hungary; >99%), and sulphuric acid (Spektrum 3D, Debrecen, Hungary; 95–97%) were used.

The investigated non-doped commercial photocatalysts were Aeroxide P25 (denoted as TiO₂-P25; produced by Evonik Industries, Essen, Germany; 90 wt% anatase, 10 wt% rutile; $D_{\text{anatase}} = 24.5$ nm, $D_{\text{rutile}} = 42$ nm), Aldrich anatase (denoted as TiO₂-AA; produced by Sigma-Aldrich, Schnelldorf, Germany; 100 wt% anatase; $D_{\text{average}} = 85$ nm), and Aldrich rutile (denoted as TiO₂-AR; produced by Sigma-Aldrich, Schnelldorf, Germany; 96 wt% rutile, 4 wt% anatase; $D_{\text{average}} \sim 315$ nm). Commercial doped TiO₂-VLP7000 (produced by Kronos Titan GmbH, Leverkusen, Germany; co-doped with nitrogen and sulphur; 100 wt% anatase; $D = 7.8$ nm) was investigated as well. The laboratory-produced TiO₂-s were visible-light-active TiO₂-N (95 wt% anatase, 5 wt% brookite; $D_{\text{anatase}} = 6.5$ nm, $D_{\text{brookite}} = 14.4$ nm; nitrogen-doped [39]) and highly UV active, non-doped TiO₂-FH (84 wt% anatase, 16 wt% ru-

tile; $D_{\text{anatase}} = 53.6 \text{ nm}$, $D_{\text{rutile}} = 69 \text{ nm}$; produced by flame hydrolysis [51]). All investigated TiO_2 -s were characterized in our previous publications [39,41,51,52].

3.2. Methods and Instrumentation

3.2.1. Photocatalytic Experiments

Phenol ($c_{\text{phenol}} = 0.1 \text{ mM}$) was applied as a model contaminant, and the concentration of the TiO_2 suspensions was $1 \text{ g}\cdot\text{L}^{-1}$. Before the experiments, the suspensions ($V = 100 \text{ mL}$) were sonicated for 5 min in the dark. From the slope of the decay curves (at $t = 0$), the initial rates (r_0) of phenol decomposition ($\text{mol}\cdot\text{dm}^{-3}\cdot\text{s}^{-1}$) were calculated using an empirical approach [52] for all TiO_2 -s and at all irradiation conditions.

Solar photocatalytic experiments were carried out as shown in Figure 4. Beakers containing photocatalyst suspensions ($V = 100 \text{ mL}$) were placed onto a multi-magnetic stirrer. They were surrounded by aluminum foil to ensure that the photocatalysts were irradiated by sunlight only from the top of the beakers and were not overshadowed by each other.

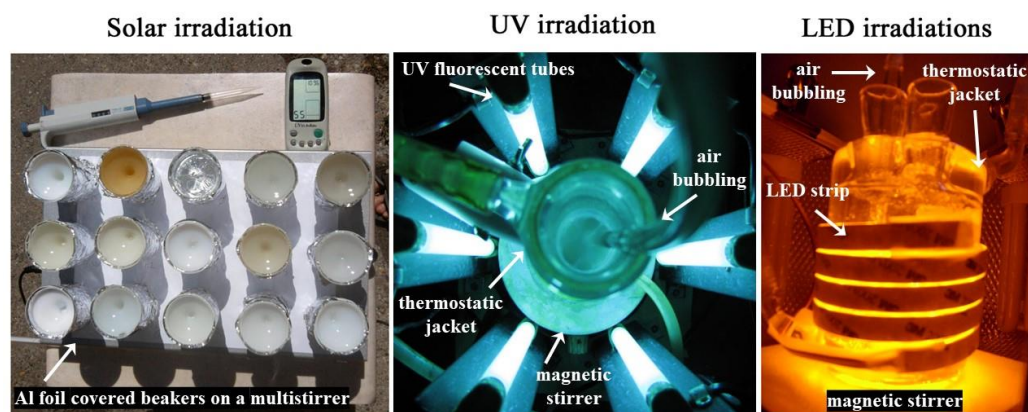


Figure 4. Applied photoreactor systems (for solar experiments, the beakers were surrounded by aluminum foil to ensure that photocatalysts were irradiated by sunlight only from the top of the beakers, which did not overshadow each other).

The UV photoreactor ($V = 100 \text{ mL}$) was a double-walled open Pyrex glass tube surrounded by a thermostatic jacket ($T = 25.0 \text{ }^\circ\text{C}$). The tube reactor (Figure 4) was irradiated by six fluorescent lamps (Vilber-Lourmat T-6L UV-A, 6W power, $\lambda_{\text{max}} = 365 \text{ nm}$). Dissolved oxygen concentration was maintained by bubbling air into the reactor.

For the measurement of photocatalytic efficiencies under visible light irradiation, an open glass vessel ($V = 100 \text{ mL}$) was applied with double walls (thermostated to $25.0 \text{ }^\circ\text{C}$). The reactor was surrounded by four conventional 24 W energy-saving compact fluorescence lamps (DÜWI 25920/R7S-24W). The spectrum of the lamp was slightly modified by circulating 1 M NaNO_2 (Molar Chemicals, Halásztelek, Hungary; min. 99.13%) aqueous solution in the thermostatic jacket. This cut-off solution absorbs UV photons below 400 nm. More details can be found in our previous publication, along with emission spectra of the compact fluorescence lamps [41]. In another series of experiments, different colored LED strips (14.4 W; 5050 SMD; 60 LED pieces within 1 m) were fixed around the reactor (Figure 4) to determine the wavelength dependence on the photocatalytic efficiencies. During LED irradiation, distilled water was circulated in the thermostatic jacket. Dissolved oxygen concentration was maintained by bubbling air into this reactor. It should be noted that the 5050 SMD LED strip was not available in violet; hence, 5 mm round violet LEDs were applied with similar geometric parameters to the 5050 SMD LED strips.

The emission spectra of the light sources were measured by an *AvaSpec-ULS 2048* spectrometer. As shown in Figure 5, the wavelength range from 300 to 650 nm was covered by the applied UV fluorescent tubes and LED strips.

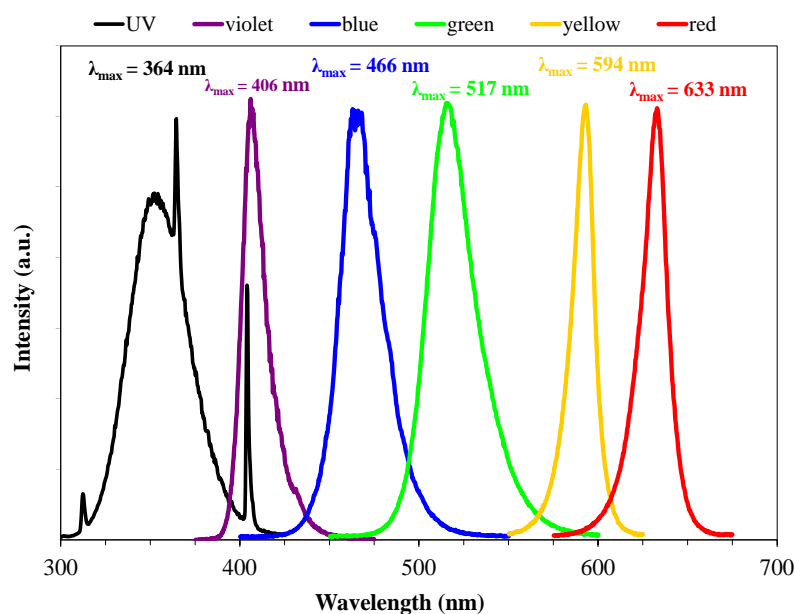
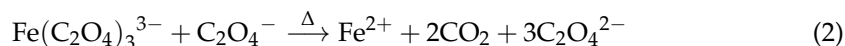
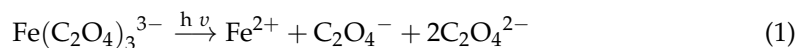


Figure 5. Emission spectra of UV-A fluorescence tubes and LED strips.

3.2.2. Potassium Ferrioxalate Actinometry

The basics of potassium ferrioxalate actinometry were developed by Hatchard and Parker in 1956 [53]. The method was optimized in 1984 by Fischer [54], and has become the most popular method for the determination of light intensity ($220 < \lambda < 550$ nm). The method is based on the stoichiometric formation of iron(II) from iron(III)-oxalate solution by photons according to the following equations:



In the presence of *o*-phenanthroline, iron(II) ions, which are formed as a result of light irradiation, yield iron(II)-triphenanthroline, which can be measured by spectrophotometry. Additional details are presented in Montalti et al. [55].

The incident photon fluxes (number of photons entered into the photoreactor) was measured as follows. First, 100 mL of potassium iron(III) oxalate solution (either 0.02 M or 0.15 M) was placed into the photoreactor. After taking the first sample (1 mL), the irradiation was turned on and five more subsequent samples were taken in the following 25–100 s. These were then injected into a dark glass flask ($V = 10$ mL) containing 6.5 mL of Milli-Q water, 2 mL of *o*-phenanthroline (0.2 wt%), and 0.5 mL of sodium acetate buffer (0.6 M Na-acetate, 0.19 M sulfuric acid). The concentration of the produced iron(II)-triphenanthroline was measured by a spectrophotometer (*Agilent 8453*) at 510 nm. The incident photon flux can be calculated by the following equation ($\text{mol}\cdot\text{s}^{-1}$):

$$I = \frac{m \times V_1 \times V_2}{V_3 \times \epsilon \times \varphi \times l} \quad (3)$$

where ' m ' is the slope of the fitted line ($m = \Delta A / \Delta t$; (s^{-1})) calculated via linear regression of the measured absorbance values; ' V_1 ' is the volume of the irradiated solution (dm^3); ' V_2 ' is the volume of the *o*-phenanthroline containing the glass flask (cm^3); ' V_3 ' is the volume of the sample taken from the photoreactor (cm^3); ' ϵ ' is the molar absorbance of iron(II)-triphenanthroline ($10,787 \text{ dm}^3\cdot\text{mol}^{-1}\cdot\text{cm}^{-1}$ at 510 nm); ' φ ' is the quantum yield of ferrioxalate actinometry at the wavelength of the applied irradiation; and ' l ' is the length of the cuvette (cm). The measurements were repeated two times under all irradiation conditions.

tions. The necessary quantum yields (φ) for the formation of iron(II) at different solution concentrations and wavelengths were provided by Fischer [54].

3.2.3. Light Intensity Measurements beyond the Ferrioxalate Method Validity Interval

Above an irradiation wavelength of 550 nm, ferrioxalate actinometry is not suitable for determining the incident photon flux. We used a photosynthetic photon flux (PPF) meter (MQ-200 Quantum meter, Apogee Instruments, Inc., Logan, Utah, USA) to calculate these values under green, yellow, and red irradiations. The sensitivity of this quantum meter is nearly constant in the visible range (400–700 nm). The light intensities of blue, green, yellow, and red LED strips were measured by the PPF meter from a fixed distance in a dark room. Then, the incident photon fluxes were calculated by multiplying the incident photon flux of blue irradiation (determined by ferrioxalate actinometry) and the ratios of light intensities measured by the PPF meter.

4. Conclusions

In this study, the wavelength dependence on the excitability of four non-doped and two doped TiO₂ photocatalysts was investigated by determining phenol decomposition rates at six different wavelength ranges. The highest determined apparent quantum yield was 1.43% under UV irradiation, for our TiO₂-FH photocatalyst synthesized by flame hydrolysis. A slightly lower value of 1.28% was determined for the reference Aeroxide P25 photocatalyst.

Under visible light irradiation, doped TiO₂-s and rutile TiO₂ showed much higher activity than Aeroxide P25 or other anatase phase non-doped TiO₂-s. The excitability of non-doped (mainly anatase phase) TiO₂-s was much better in the UV range than that of the doped TiO₂-s. Kronos VLP7000 could be excited in the whole UV–vis spectrum, although the apparent quantum yields were 1–2 order(s) of magnitude lower in the visible range than in the UV range. This resulted in higher performance for non-doped TiO₂-s under solar light utilization despite the order of magnitude lower quantity of the UV photons in solar light.

Our results highlight that enhancing the excitability of a photocatalyst in the visible range is not necessarily associated with greater photocatalytic activity in solar applications. For visible-light-active photocatalysts, better optical properties and enhanced quantum yield in the visible light range can be overcompensated by a low quantum yield in the UV range, which can lead to lower overall photocatalytic performance. Therefore, UV excitability is crucial during the development of novel solar-active photocatalysts, and must be described alongside visible light activity. Alternatively, carrying out outdoor solar experiments or using solar light simulators is recommended for evaluating the performance of novel photocatalysts developed for solar-cleanable membrane surfaces, artificial synthesis, and other sunlight-based processes.

Naturally, visible light excitability is the only essential property for indoor applications because of the absence of UV photons. Therefore, visible light irradiation may be sufficient for photocatalytic experiments in such cases.

Author Contributions: G.V.: Supervision, Writing—original draft, Investigation, Conceptualization, Funding acquisition. T.G.: Writing—review and editing. O.V.: Investigation. T.A.: Writing—review and editing. K.H.: Conceptualization, Writing—review and editing. Z.P.: Writing—review and editing, Conceptualization. All authors have read and agreed to the published version of the manuscript.

Funding: This research was funded by the Hungarian National Research, Development and Innovation Office—NKFIH (FK_20_135202). The authors are indebted to Evonik Industries and for Kronos GmbH for supporting our work by supplying the reference TiO₂-s.

Data Availability Statement: Data are contained within the article.

Conflicts of Interest: The authors declare no conflict of interest.

References

1. Menéndez-Flores, V.M.; Bahnemann, D.W.; Ohno, T. Visible light photocatalytic activities of S-doped TiO₂-Fe³⁺ in aqueous and gas phase. *Appl. Catal. B* **2011**, *103*, 99–108. [CrossRef]
2. Li, X.; Liu, Y.; Yang, P.; Shi, Y. Visible light-driven photocatalysis of W, N co-doped TiO₂. *Particuology* **2013**, *11*, 732–736. [CrossRef]
3. Kumar, S.; Bhawna; Sharma, R.; Gupta, A.; Dubey, K.K.; Khan, A.M.; Singhal, R.; Kumar, R.; Bharti, A.; Singh, P.; et al. TiO₂ based Photocatalysis membranes: An efficient strategy for pharmaceutical mineralization. *Sci. Total Environ.* **2022**, *845*, 157221. [CrossRef]
4. Pelosato, R.; Bolognino, I.; Fontana, F.; Sora, I.N. Applications of Heterogeneous Photocatalysis to the Degradation of Oxytetracycline in Water: A Review. *Molecules* **2022**, *27*, 2743. [CrossRef] [PubMed]
5. Mahmood, A.; Muhmood, T.; Ahmad, F. Carbon nanotubes heterojunction with graphene like carbon nitride for the enhancement of electrochemical and photocatalytic activity. *Mater. Chem. Phys.* **2022**, *278*, 125640. [CrossRef]
6. Muhmood, T.; Xia, M.; Lei, W.; Wang, F. Under vacuum synthesis of type-I heterojunction between red phosphorus and graphene like carbon nitride with enhanced catalytic, electrochemical and charge separation ability for photodegradation of an acute toxicity category-III compound. *Appl. Catal. B* **2018**, *238*, 568–575. [CrossRef]
7. Santos, E.N.; Ágoston, Á.; Kertész, S.; Hodúr, C.; László, Z.; Pap, Z.; Kása, Z.; Alapi, T.; Krishnan, S.A.G.; Arthanareeswaran, G.; et al. Investigation of the applicability of TiO₂, BiVO₄, and WO₃ nanomaterials for advanced photocatalytic membranes used for oil-in-water emulsion separation. *Asia-Pac. J. Chem. Eng.* **2020**, *15*, e2549.
8. Nascimbén Santos, É.; László, Z.; Hodúr, C.; Arthanareeswaran, G.; Veréb, G. Photocatalytic membrane filtration and its advantages over conventional approaches in the treatment of oily wastewater: A review. *Asia-Pac. J. Chem. Eng.* **2020**, *15*, e2533. [CrossRef]
9. Zarghami, S.; Mohammadi, T.; Sadrzadeh, M.; Van der Bruggen, B. Superhydrophilic and underwater superoleophobic membranes—A review of synthesis methods. *Prog. Polym. Sci.* **2019**, *98*, 101166. [CrossRef]
10. Mogyrosi, K.; Kmetyko, A.; Czirbus, N.; Vereb, G.; Sipos, P.; Dombi, A. Comparison of the substrate dependent performance of Pt-, Au- and Ag-doped TiO₂ photocatalysts in H₂-production and in decomposition of various organics. *React. Kinet. Catal. Lett.* **2009**, *98*, 215–225. [CrossRef]
11. Escobedo, S.; de Lasa, H. Synthesis and Performance of Photocatalysts for Photocatalytic Hydrogen Production: Future Perspectives. *Catalysts* **2021**, *11*, 1505. [CrossRef]
12. Corredor, J.; Rivero, M.J.; Rangel, C.M.; Gloaguen, F.; Ortiz, I. Comprehensive review and future perspectives on the photocatalytic hydrogen production. *J. Chem. Technol. Biotechnol.* **2019**, *94*, 3049–3063. [CrossRef]
13. Hu, J.D.; Cao, Y.L.; Wang, K.; Jia, D.Z. Green solid-state synthesis and photocatalytic hydrogen production activity of anatase TiO₂ nanoplates with super heat-stability. *RSC Adv.* **2017**, *7*, 11827–11833. [CrossRef]
14. Bojinova, A.; Kaneva, N.; Papazova, K.; Elias, A.; Stoyanova-Elias, E.; Dimitrov, D. Green synthesis of UV and visible light active TiO₂/WO₃ powders and films for malachite green and ethylene photodegradation. *React. Kinet. Mech. Catal.* **2017**, *120*, 821–832. [CrossRef]
15. Serpone, N. Heterogeneous Photocatalysis and Prospects of TiO₂-Based Photocatalytic DeNO_xing the Atmospheric Environment. *Catalysts* **2018**, *8*, 553. [CrossRef]
16. Wu, D.; Wang, L.; Song, X.; Tan, Y. Enhancing the visible-light-induced photocatalytic activity of the self-cleaning TiO₂-coated cotton by loading Ag/AgCl nanoparticles. *Thin Solid Films* **2013**, *540*, 36–40. [CrossRef]
17. Soklič, A.; Tasbihi, M.; Kete, M.; Štangar, U.L. Deposition and possible influence of a self-cleaning thin TiO₂/SiO₂ film on a photovoltaic module efficiency. *Catal. Today* **2015**, *252*, 54–60. [CrossRef]
18. Tallósy, S.P.; Janovák, L.; Ménesi, J.; Nagy, E.; Juhász, Á.; Balázs, L.; Deme, I.; Buzás, N.; Dékány, I. Investigation of the antibacterial effects of silver-modified TiO₂ and ZnO plasmonic photocatalysts embedded in polymer thin films. *Environ. Sci. Pollut. Res.* **2014**, *21*, 11155–11167. [CrossRef]
19. Arunachalam, P.; Nagai, K.; Amer, M.S.; Ghanem, M.A.; Ramalingam, R.J.; Al-Mayouf, A.M. Recent Developments in the Use of Heterogeneous Semiconductor Photocatalyst Based Materials for a Visible-Light-Induced Water-Splitting System—A Brief Review. *Catalysts* **2021**, *11*, 160. [CrossRef]
20. Ma, J.; Chu, L.; Guo, Y.; Sun, C.; Yan, H.; Li, Z.; Li, M. Graphene Quantum Dots Improved “Caterpillar”-like TiO₂ for Highly Efficient Photocatalytic Hydrogen Production. *Materials* **2021**, *14*, 5354. [CrossRef]
21. Nguyen, V.-H.; Nguyen, B.-S.; Jin, Z.; Shokouhimehr, M.; Jang, H.W.; Hu, C.; Singh, P.; Raizada, P.; Peng, W.; Shiung Lam, S.; et al. Towards artificial photosynthesis: Sustainable hydrogen utilization for photocatalytic reduction of CO₂ to high-value renewable fuels. *Chem. Eng. J.* **2020**, *402*, 126184. [CrossRef]
22. He, J.; Janaky, C. Recent Advances in Solar-Driven Carbon Dioxide Conversion: Expectations versus Reality. *ACS Energy Lett.* **2020**, *5*, 1996–2014. [CrossRef] [PubMed]
23. Qamar, M.; Merzougui, B.; Anjum, D.; Hakeem, A.S.; Yamani, Z.H.; Bahnemann, D. Synthesis and photocatalytic activity of mesoporous nanocrystalline Fe-doped titanium dioxide. *Catal. Today* **2014**, *230*, 158–165. [CrossRef]
24. Ansari, S.A.; Khan, M.M.; Ansari, M.O.; Cho, M.H. Nitrogen-doped titanium dioxide (N-doped TiO₂) for visible light photocatalysis. *New J. Chem.* **2016**, *40*, 3000–3009. [CrossRef]

25. Li, Y.; Li, M.; Xu, P.; Tang, S.; Liu, C. Efficient photocatalytic degradation of acid orange 7 over N-doped ordered mesoporous titania on carbon fibers under visible-light irradiation based on three synergistic effects. *Appl. Catal. A Gen.* **2016**, *524*, 163–172. [[CrossRef](#)]
26. Ahmed, S.; Rasul, M.G.; Brown, R.; Hashib, M.A. Influence of parameters on the heterogeneous photocatalytic degradation of pesticides and phenolic contaminants in wastewater: A short review. *J. Environ. Manag.* **2011**, *92*, 311–330. [[CrossRef](#)]
27. Ohtani, B. Titania Photocatalysis beyond Recombination: A Critical Review. *Catalysts* **2013**, *3*, 942–953. [[CrossRef](#)]
28. Nosaka, Y.; Nosaka, A.Y. Langmuir-Hinshelwood and Light-Intensity Dependence Analyses of Photocatalytic Oxidation Rates by Two-Dimensional-Ladder Kinetic Simulation. *J. Phys. Chem. C* **2018**, *122*, 28748–28756. [[CrossRef](#)]
29. Nafradi, M.; Alapi, T.; Bencsik, G.; Janaky, C. Impact of Reaction Parameters and Water Matrices on the Removal of Organic Pollutants by TiO₂/LED and ZnO/LED Heterogeneous Photocatalysis Using 365 and 398 nm Radiation. *Nanomaterials* **2021**, *12*, 5. [[CrossRef](#)]
30. Nafradi, M.; Alapi, T.; Farkas, L.; Bencsik, G.; Kozma, G.; Hernadi, K. Wavelength Dependence of the Transformation Mechanism of Sulfonamides Using Different LED Light Sources and TiO₂ and ZnO Photocatalysts. *Materials* **2021**, *15*, 49. [[CrossRef](#)]
31. Banerjee, S.; Gopal, J.; Muraleedharan, P.; Tyagi, A.; Rai, B. Physics and chemistry of photocatalytic titanium dioxide: Visualization of bactericidal activity using atomic force microscopy. *Curr. Sci.* **2005**, *90*, 1378–1383.
32. Rengifo-Herrera, J.A.; Pierzchała, K.; Sienkiewicz, A.; Forró, L.; Kiwi, J.; Pulgarin, C. Abatement of organics and Escherichia coli by N, S co-doped TiO₂ under UV and visible light. Implications of the formation of singlet oxygen (¹O₂) under visible light. *Appl. Catal. B* **2009**, *88*, 398–406. [[CrossRef](#)]
33. Iwase, M.; Yamada, K.; Kurisaki, T.; Prieto-Mahaney, O.O.; Ohtani, B.; Wakita, H. Visible-light photocatalysis with phosphorus-doped titanium(IV) oxide particles prepared using a phosphide compound. *Appl. Catal. B* **2013**, *132–133*, 39–44. [[CrossRef](#)]
34. Myilsamy, M.; Murugesan, V.; Mahalakshmi, M. Indium and cerium co-doped mesoporous TiO₂ nanocomposites with enhanced visible light photocatalytic activity. *Appl. Catal. A Gen.* **2015**, *492*, 212–222. [[CrossRef](#)]
35. Nishiyama, N.; Kozasa, K.; Yamazaki, S. Photocatalytic degradation of 4-chlorophenol on titanium dioxide modified with Cu(II) or Cr(III) ion under visible light irradiation. *Appl. Catal. A Gen.* **2016**, *527*, 109–115. [[CrossRef](#)]
36. Wu, P.; Xie, R.; Imlay, J.A.; Shang, J.K. Visible-light-induced photocatalytic inactivation of bacteria by composite photocatalysts of palladium oxide and nitrogen-doped titanium oxide. *Appl. Catal. B* **2009**, *88*, 576–581. [[CrossRef](#)] [[PubMed](#)]
37. Rengifo-Herrera, J.A.; Kiwi, J.; Pulgarin, C. N, S co-doped and N-doped Degussa P-25 powders with visible light response prepared by mechanical mixing of thiourea and urea. Reactivity towards E. coli inactivation and phenol oxidation. *J. Photochem. Photobiol. A* **2009**, *205*, 109–115. [[CrossRef](#)]
38. Rengifo-Herrera, J.A.; Pulgarin, C. Photocatalytic activity of N, S co-doped and N-doped commercial anatase TiO₂ powders towards phenol oxidation and E. coli inactivation under simulated solar light irradiation. *Solar Energy* **2010**, *84*, 37–43. [[CrossRef](#)]
39. Pap, Z.; Baia, L.; Mogyorosi, K.; Dombi, A.; Oszko, A.; Danciu, V. Correlating the visible light photoactivity of N-doped TiO₂ with brookite particle size and bridged—Nitro surface species. *Catal. Commun.* **2011**, *17*, 1–7. [[CrossRef](#)]
40. Dolat, D.; Mozia, S.; Ohtani, B.; Morawski, A.W. Nitrogen, iron-single modified (N-TiO₂, Fe-TiO₂) and co-modified (Fe, N-TiO₂) rutile titanium dioxide as visible-light active photocatalysts. *Chem. Eng. J.* **2013**, *225*, 358–364. [[CrossRef](#)]
41. Veréb, G.; Manczinger, L.; Bozsó, G.; Sienkiewicz, A.; Forró, L.; Mogyorósi, K.; Hernádi, K.; Dombi, A. Comparison of the photocatalytic efficiencies of bare and doped rutile and anatase TiO₂ photocatalysts under visible light for phenol degradation and E. coli inactivation. *Appl. Catal. B* **2013**, *129*, 566–574. [[CrossRef](#)]
42. Emeline, A.V.; Zhang, X.; Jin, M.; Murakami, T.; Fujishima, A. Spectral dependences of the activity and selectivity of N-doped TiO₂ in photodegradation of phenols. *J. Photochem. Photobiol. A* **2009**, *207*, 13–19. [[CrossRef](#)]
43. Wang, Z.; Cai, W.; Hong, X.; Zhao, X.; Xu, F.; Cai, C. Photocatalytic degradation of phenol in aqueous nitrogen-doped TiO₂ suspensions with various light sources. *Appl. Catal. B* **2005**, *57*, 223–231. [[CrossRef](#)]
44. Antonopoulou, M.; Giannakas, A.; Bairamis, F.; Papadaki, M.; Konstantinou, I. Degradation of organophosphorus flame retardant tris (1-chloro-2-propyl) phosphate (TCPP) by visible light N, S-codoped TiO₂ photocatalysts. *Chem. Eng. J.* **2016**, *318*, 231–239. [[CrossRef](#)]
45. Song, S.; Tu, J.J.; He, Z.Q.; Hong, F.Y.; Liu, W.P.; Chen, J.M. Visible light-driven iodine-doped titanium dioxide nanotubes prepared by hydrothermal process and post-calcination. *Appl. Catal. A* **2010**, *378*, 169–174. [[CrossRef](#)]
46. He, Z.Q.; Wang, C.; Wang, H.Y.; Hong, F.Y.; Xu, X.H.; Chen, J.M.; Song, S. Increasing the catalytic activities of iodine doped titanium dioxide by modifying with tin dioxide for the photodegradation of 2-chlorophenol under visible light irradiation. *J. Hazard. Mater.* **2011**, *189*, 595–602. [[CrossRef](#)]
47. He, Z.Q.; Zhan, L.Y.; Hong, F.Y.; Song, S.; Lin, Z.Y.; Chen, J.M.; Jin, M.T. A visible light-responsive iodine-doped titanium dioxide nanosphere. *J. Environ. Sci.-China* **2011**, *23*, 166–170. [[CrossRef](#)]
48. Veréb, G.; Manczinger, L.; Oszkó, A.; Sienkiewicz, A.; Forró, L.; Mogyorósi, K.; Dombi, A.; Hernádia, K. Highly efficient bacteria inactivation and phenol degradation by visible light irradiated iodine doped TiO₂. *Appl. Catal. B* **2013**, *129*, 194–201.
49. Guo, S.; Han, S.; Haifeng, M.; Zeng, C.; Sun, Y.; Chi, B.; Pu, J.; Li, J. Synthesis of phosphorus-doped titania with mesoporous structure and excellent photocatalytic activity. *Mater. Res. Bull.* **2013**, *48*, 3032–3036. [[CrossRef](#)]
50. Thind, S.S.; Wu, G.; Chen, A. Synthesis of mesoporous nitrogen–tungsten co-doped TiO₂ photocatalysts with high visible light activity. *Appl. Catal. B* **2012**, *111–112*, 38–45. [[CrossRef](#)]

51. Balazs, N.; Sranko, D.F.; Dombi, A.; Sipos, P.; Mogyorosi, K. The effect of particle shape on the activity of nanocrystalline TiO₂ photocatalysts in phenol decomposition. Part 2: The key synthesis parameters influencing the particle shape and activity. *Appl. Catal. B* **2010**, *96*, 569–576. [[CrossRef](#)]
52. Veréb, G.; Ambrus, Z.; Pap, Z.; Kmetykó, Á.; Dombi, A.; Danciu, V.; Cheesman, A.; Mogyorósi, K. Comparative study on UV and visible light sensitive bare and doped titanium dioxide photocatalysts for the decomposition of environmental pollutants in water. *Appl. Catal. A Gen.* **2012**, *417–418*, 26–36. [[CrossRef](#)]
53. Hatchard, C.G.; Parker, C.A. A new sensitive chemical actinometer-II. Potassium ferrioxalate as a standard chemical actinometer. *Proc. R. Soc. Lond. Ser. A Math. Phys. Sci.* **1956**, *A235*, 518–536.
54. Fischer, E. Ferri-oxalate actinometry. *Newsletters* **1984**, *21*, 33–34.
55. Montalti, M.; Credi, A.; Prodi, L.; Gandolfi, M.T. *Handbook of Photochemistry*, 3rd ed.; Taylor & Francis Group: Abingdon, UK, 2006.